THE JOURNAL OF PHYSICAL CHEMISTRY A

 VOLUME 109, NUMBER 22, JUNE 9, 2005

ARTICLES

Influence of a Weak Hydrogen Bond on Vibrational Coherence Probed by Photon Echoes in DCl Dimer Trapped in Solid Nitrogen

M. Broquier,[†] C. Crépin,*[,†] A. Cuisset,[†,‡] H. Dubost,[†] and J. P. Galaup[§]

Laboratoire de Photophysique Moléculaire du CNRS, Bât 210, Université Paris-Sud, 91405 Orsay Cedex, France, and Laboratoire Aimé Cotton, CNRS, Bât 505, Université Paris-Sud, 91405 Orsay Cedex, France

Received: February 25, 2005; In Final Form: April 15, 2005

The dynamics in the ground electronic state of the two intramolecular D-Cl stretching modes of $(DCl)_2$ in nitrogen solid has been probed by degenerate four wave mixing experiments. Accumulated photon echoes on the "free" ν_1 and "bonded" ν_2 modes have been performed by means of the free electron laser of Orsay (CLIO). The analysis of the time-resolved signals provides information on the various processes responsible for the loss of vibrational coherence, in particular intra- and intermolecular vibrational energy transfer and pure dephasing. The influence of the weak hydrogen bond is clearly observed on the coherence times of the two stretching modes. Whatever the temperature, the homogeneous width of ν_2 lines is almost twice that of ν_1 lines. Contrary to the case of isolated DCl trapped in solid nitrogen, no obvious effect of the nitrogen lattice can be extracted from the temperature dependence of the coherence times.

1. Introduction

Vibrational phase relaxation is known to be a powerful probe of the intermolecular interactions in the condensed phase.[1] The linear absorption spectrum of a vibrational transition contains all contributions from dynamics occurring over different time scales covering the whole range relevant to the interactions between the molecular system and its environment. However, the inhomogeneous contribution often dominates the line shape of the linear absorption spectrum, masking the precise nature of the interactions between an oscillator and its environment. For more than 20 years, several nonlinear spectroscopic tools have been used to eliminate the inhomogeneous broadening and to recover the homogeneous spectrum. Such inhomogeneous free methods are spectral hole burning in frequency domain and photon echoes in time domain.[2−4] More recently, the development of ultrafast infrared lasers has allowed the time-resolved observation of vibrational dephasing by means of nonlinear experiments.[5−8] IR photon echoes are capable of extracting the homogeneous contribution, related to the dephasing time (or coherence time) T_2 by the well-known relation: $\pi\Gamma_{hom} = T_2^{-1} = (2T_1)^{-1} + T_2^{*-1}$ where T_1 and T_2^* represent the vibrational population and the pure dephasing lifetimes, respectively.

In this paper, photon echoes, applied to the DCl dimer trapped in solid nitrogen, allow the influence of a weak hydrogen bond on the vibrational dynamics of the intramolecular modes to be investigated. Usually, hydrogen bond formation leads to the observation of a spectral broadening: the bandwidth of a hydrogen-bonded vibration is typically 1 order of magnitude larger than the corresponding vibration in the uncomplexed

* To whom correspondence should be addressed. E-mail: claudine.crepin-gilbert@ppm.u-psud.fr.
[†] Laboratoire de Photophysique Moléculaire du CNRS.
[‡] Present address: Laboratoire de Physico-Chimie de l'Atmosphère CNRS UMR 8101, Université du Littoral Côte d'Opale, 189 A Ave. Maurice Schumann 59140 Dunkerque, France.
[§] Laboratoire Aimé Cotton, CNRS.

10.1021/jp0509921 CCC: $30.25
Published on Web 05/17/2005

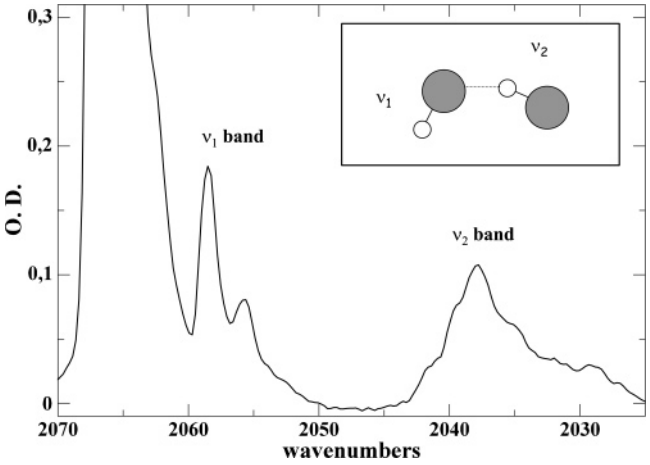

Figure 1. FTIR spectrum of DCl in the dimer region at $T = 7.7$ K, $c = 1.3\%$ ([DCl]/[N_2] = 0.8%). In the insert, a sketch of the dimer geometry is shown and the two intramolecular vibrations are indicated.

molecule, suggesting that the hydrogen bond strongly changes the vibrational dephasing rate. In the condensed phase, the two main theoretical models considered in the literature to explain the dephasing in hydrogen-bonded systems are based on the anharmonic coupling between the intramolecular (XH) and the intermolecular (XH···Y) stretching modes, like in the gas phase.[9,10] In one model, the relaxation is directly connected to the coupling between the fluctuating local electric field and the dipole moment of the complex. Fluctuations result in a broadening of the spectrum proportional to $(\partial\mu/\partial r)$ where r is the XH separation.[11] The other model involves an indirect mechanism where the relaxation takes place via the coupling of the (XH) and the (XH···Y) modes along the X−H coordinate. The coherence of the XH···Y mode is lost by coupling with the surrounding molecules (the bath), affecting the phase of the XH vibration.[12−14]

The H(D)Cl dimer, like the HF dimer, is considered as a model of weakly hydrogen bonded complexes, and for this reason, numerous sophisticated experimental and theoretical studies in the gas phase have been performed on this system. Gas-phase infrared spectroscopic measurements in long path cell[15−17] and molecular beam[18−21] show that the complex has a nearly perpendicular geometry, the H-bonded proton being slightly off the axis between the chlorine atoms, by 16°, whereas the angle between this axis and the "free" proton is 87°.[18] A sketch of the dimer geometry is shown in the insert of Figure 1. The two D-Cl stretching modes are almost localized on the two D-Cl bonds, and the only difference between them comes from the influence of the hydrogen bond since one H(D)Cl group is acting as the proton acceptor ("free" H(D)Cl), whereas the other is the proton donor ("bonded" H(D)Cl). Hence, the hydrogen bond affects the frequencies, the lifetimes and the transition dipole moment of both vibrations but not in the same manner. Both intramolecular vibrations are downshifted ($\Delta\nu$) from the monomer frequency. The vibration ν_1 corresponds to the "free" stretch with $\Delta\nu_1 = 11.7$ and 9.1 cm^{-1} for $(HCl)_2$ and $(DCl)_2$, respectively. The vibration ν_2 corresponds to the "bonded" stretch with $\Delta\nu_2 = 38.0$ and 28.6 cm^{-1} for $(HCl)_2$ and $(DCl)_2$, respectively.[18,19] Gas-phase vibrational predissociation lifetimes for $(HCl)_2$ have been deduced from slit jet experiments.[18] The $\upsilon = 1$ level of the mode ν_2 yielded a value T_1 of 31 ns. For the $\upsilon = 1$ level of the mode ν_1, a lower limit $T_1 > 100$ns was established. Similar line widths measurements for $(DCl)_2$ gave $T_1 > 3$ ns, at the experimental resolution limit. The lifetimes of both $(HCl)_2$ stretching modes have also been measured in photofragmentation experiments,[22] leading to slightly different values: $T_1 = 48$ ns for the free mode and $T_1 = 28$ ns for the bonded mode. An intensity enhancement of the rotationally resolved lines of the ν_2 band compared to the ν_1 band is observed. A $I_{\nu 2}/I_{\nu 1}$ absorption intensity ratio around 5 is deduced from the slit jet spectra.[19]

Numerous studies have also been performed in the condensed phase, especially in van der Waals solids.[23−28] In this paper, the nitrogen matrix is chosen as the solid environment, to compare with our previous study on monomers.[29] The spectroscopy is well-known, but the lifetimes of $(DCl)_2$ vibrations have not been measured. In solid nitrogen, the host and guest are of similar size so that H(D)Cl molecules occupy a single substitutional site of the N_2 fcc lattice. In addition, no rotation of the H(D)Cl species occurs. A dimer is formed when two molecules are in the nearest neighbor situation, the nearest neighbor distance in the nitrogen lattice being quite comparable to the distance between the two H(D)Cl molecules in the free dimer. The equilibrium geometry of the dimer has been calculated by Girardet et al.[24] The equilibrium configuration of the two molecules is found to be nearly orthogonal and nonplanar, the internuclear axes being located in the planes perpendicular to the substituted N_2 molecules. The two D-Cl stretching mode frequencies are downshifted from the monomer frequency in solid nitrogen: $\Delta\nu_1 = 8.4$ cm^{-1} and $\Delta\nu_2 = 29.2$ cm^{-1} for ν_1 and ν_2, respectively; that is, the shifts are very similar to those measured in the gas phase. In addition, the interaction between the dimer and the solid leads to a vibrational frequency shift from the gas-phase value: like in the monomer case both stretching modes are downshifted by almost 24 cm^{-1} from the gas phase. Thus, the shift induced by the nitrogen matrix is of the same order of magnitude as the shift induced by the hydrogen bond in the bonded mode. The intensity ratio $I_{\nu 2}/I_{\nu 1}$ is around 1.5, deduced from the $(HCl)_2$ and $(DCl)_2$ spectra.[28] The difference between this ratio in the condensed phase and in the gas phase is related to the specific N_2 matrix effect. As a matter of fact, our previous studies on the monomer have demonstrated an enhancement of the vibrational transition dipole moment of DCl in nitrogen solid compared with the gas-phase value.[29]

2. Experimental Setup

Infrared degenerate four wave mixing experiments on DCl were performed using the CLIO Free Electron Laser[30,31] as the laser source. The choice of the deuterated species was imposed by the laser spectral range. The excitation energy was tuned between 2030 and 2060 cm^{-1} with a typical spectral width around 20 cm^{-1}. The average laser power was 200 mW. The CLIO FEL has a specific time sequence: subpicosecond pulses are supplied at a rate of 62.5 MHz in bunches of 10 μs, and the repetition rate of bunches is 25 Hz. The DFWM experimental setup was a two pulse photon echo configuration and has been described in details elsewhere.[7] Due to the short delay between the pulses within a bunch ($T_r = 16$ ns), the same experimental setup allowed to record accumulated photon echoes when the vibrational lifetime of the probed oscillator was longer than T_r:[8] the interaction of the first two pulses (wavevectors $\mathbf{k}_1$ and $\mathbf{k}_2$) created a population grating in the sample, with a lifetime T_1, so that the following pulse in the bunch in the direction $\mathbf{k}_2$, delayed by T_r from the second pulse, can act on the grating, generating a stimulated three pulse photon echo, in the same direction as the two pulse photon echo. When no data on the time T_1 were available, a detailed analysis of the recorded signal was necessary to determine whether two pulse or stimulated

TABLE 1: Vibrational Transition Frequencies of DCl Monomers and Dimers in N_2 Matrices at $T = 7.5$ K, $c = 0.2\%$, $[DCl]/[N_2] = 0.13\%$

wavenumbers (cm^{-1})	assignments	
2067.7	$D^{35}Cl$ monomer	
2066.0	$D^{35}Cl$ *nnn* dimer[a]	
2064.7	$D^{37}Cl$ monomer	
2063.4	$D^{37}Cl$ *nnn* dimer[a]	
2058.6	$D^{35}Cl-H^{35-37}Cl$	mode ν_1
2058.6	$D^{35}Cl$-$D^{35-37}Cl$	
2055.7	$D^{37}Cl-H^{35-37}Cl$	
2055.7	$D^{37}Cl$-$D^{35-37}Cl$	
2039.5	$H^{35-37}Cl$-$D^{35}Cl$	mode ν_2
2037.8	$D^{35-37}Cl$-$D^{35}Cl$	
2036.8	$H^{35-37}Cl$-$D^{37}Cl$	
2034.8	$D^{35-37}Cl$-$D^{37}Cl$	

[a] DCl molecules in position of *n* ext *n* earest *n* eighbours (*nnn*) in the fcc lattice.[24]

photon echoes were observed. In particular, a nonzero DFWM signal at negative delay times between the first two pulses was a signature of the presence of stimulated photon echoes. The temporal resolution of our experiments was in the range 0.6−1.5 ps depending on the setting of the FEL.[29,32]

DCl was obtained from Merck Sharp Dohme Isotopes. Experiments were carried out using a liquid helium bath cryostat (Air Liquide) with a minimum temperature of 7 K. The gas mixture DCl/HCl/N_2, with different concentrations $c = [DCl+HCl]/[N_2]$ ($c \leq 1.3\%$), was deposited on a cold sapphire window maintained at 20 K. Although the variable desorption of H(D)Cl in the stainless steel vacuum line makes exact concentration determination difficult, a DCl/HCl ratio of about 3 was targeted. Nevertheless, the presence of both isotopic species makes the absorption spectra complex. The final composition of the solid samples was checked and analyzed by measuring absorption spectra by means of a Mattson FTIR spectrometer with a resolution of 0.25 cm^{-1}. From the absorption spectra, the ratio [DCl]/[HCl] and thus the concentration $[DCl]/[N_2]$ were estimated.

3. Results

3.1. Absorption. The spectrum observed after deposition is dominated by the absorption bands of the monomers between 2070 and 2060 cm^{-1}, and the bands assigned to the dimers appear on the red side around 2058 and 2039 cm^{-1} (Figure 1). The presence of HCl and of the isotopic species of chlorine atoms leads to the formation of 16 isotopic dimers, i.e., to the observation of 32 H(D)-Cl stretching modes. In the D-Cl spectral region, each dimer absorption band is composed of eight lines coming from different combinations of monomer isotopes. The spectral shift due to the different chlorine isotopic species of the complexation partner of the observed (free or bonded) D-Cl is very weak, so the broad dimer absorption bands of the two stretching modes are analyzed in terms of four different components.

The spectral analysis is first performed on a diluted sample ($c = 0.2\%$) in order to obtain precise values of the vibrational frequencies. A crude decomposition in four lines with Lorentzian profiles[33] of each stretching band gives an estimation of the line widths $\delta\nu$ of each component. The measured frequencies and corresponding assignments are summarized in Table 1. Only two lines are observed in the ν_1 band with relative intensities correlated to the natural abundance of isotopic chlorine atoms, whereas the analysis of the ν_2 band in the H−Cl region clearly reveals the presence of DCl−HCl mixed dimers. In fact, the

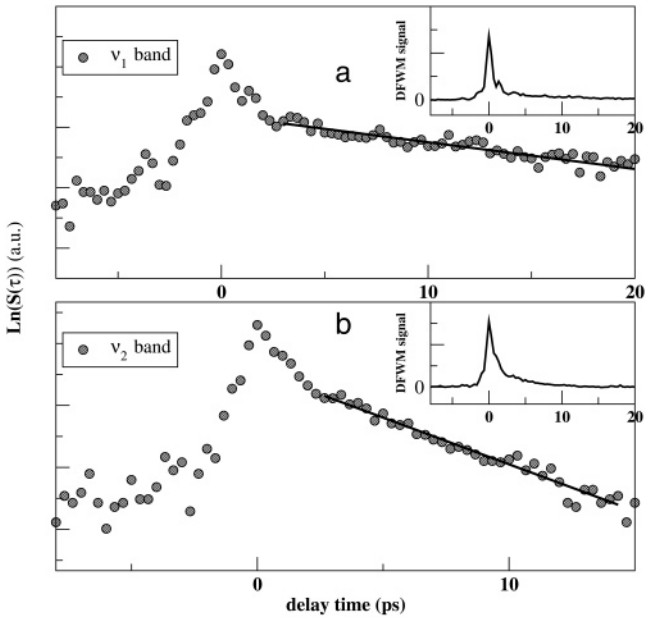

Figure 2. Semi logarithm plot of the DFWM signal intensity vs delay time τ for selective excitation of ν_1 band [$\nu_{laser} = 2053$ cm^{-1}, $\delta\nu_{laser} \leq 15$ cm^{-1}] (a) and ν_2 band [$\nu_{laser} = 2036$ cm^{-1}, $\delta\nu_{laser} \leq 15$ cm^{-1}] (b). In the inserts, typical experimental DFWM signals are shown. The sample temperature is 10 K, $c = 1.3\%$.

DCl-DCl and DCl−HCl dimers have the same free mode frequencies, as reported elsewhere[24] for the ^{35}Cl isotopic species (a similar decomposition of the ν_1 band in the H−Cl region gives four different frequencies[35]).

The line widths of all the four components of the ν_2 band seem to be always larger than those of the ν_1 band, as also observed in the H−Cl region. These line widths increase with the concentration, but $\delta\nu_1 < \delta\nu_2$ is verified whatever the concentration and the temperature of the sample, for each component and for the total spectral width of the bands. At the concentration $c = 1.3\%$ of the samples used in the DFWM experiments, $\delta\nu_1 = 1.6$ cm^{-1} and $\delta\nu_2 = 2.8$ cm^{-1}, with total widths of 3.7 and 6.0 cm^{-1} for the ν_1 and the ν_2 bands, respectively, at $T = 7.5$ K. No temperature dependence is observed for the ν_2 band, whereas at low concentration ($c = 0.2\%$), there is a weak reversible temperature dependence for $\delta\nu_1$: $\delta\nu_1$ increases from 0.8 cm^{-1} at 7.5 K to 1.1 cm^{-1} at $T = 15$ K. Such a reversibility indicates that the homogeneous contribution is non-negligible in this last case. However, at higher concentrations, the inhomogeneous broadening dominates the absorption profile of the ν_1 band, which is always verified for the ν_2 band. No conclusion on the homogeneous widths of any of the vibrational stretching modes of the dimers can be drawn from these investigations in the spectral domain.

3.2. Infrared Degenerate Four Wave Mixing Signals. The time-resolved DFWM signals exhibit very different behaviors depending on the frequency and spectral width of the laser.[32] In most cases, two components are clearly observed: (i) an oscillating structure around the zero temporal delay associated with a short component and (ii) a long and weak component, corresponding to the rephasing process, involving the coherence time of the excited transitions. Examples of signals are reported in the inserts of Figure 2. The presence of these two components reflects a partial spectral diffusion behavior,[8] occurring when rephasing processes are possible only for a fraction of the initially excited oscillators. Due to the collective excitation of the species included in the laser spectral width, the periodic time structure is related to the frequency differences between

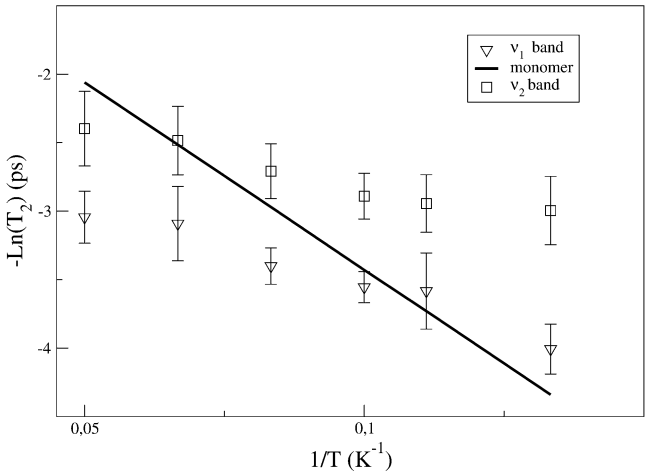

Figure 3. T_2 time vs temperature for the ν_1 and ν_2 bands of the DCl dimer. The full line represents the behavior of time T_2 of the monomer band.[29]

all the excited transitions.[29,34] The short time period involved in most of the signals corresponds to the frequency difference between the two stretching modes of the dimer.

A particular behavior is observed when the laser emission is between the vibrational monomer frequency and ν_1: only the short component is observed and the oscillation time period is related to the frequency difference between the monomer and the ν_1 band. The study of monomers showed that the spectral diffusion is very efficient between monomers at the concentration of the samples of interest,[29] moreover the inhomogeneous absorption band of monomers overlaps that of dimers in this spectral region (see Figure 1). In this case, the nonlinear signal reflects only a very efficient spectral diffusion due to fast vibrational energy transfers between the quasiresonant stretching mode of monomers and the free mode of the dimers.[32] This case will not be discussed further.

The dephasing time T_2 is included in the long time component of the DFWM signal (see part 4.1), which clearly depends on the frequency of the excitation laser. This component is longer when the FEL is tuned on the ν_1 band than when it is tuned on the ν_2 band. For the measurement of the time T_2, we select DFWM signals with no significant oscillations in order to avoid collective excitations (see Figure 2). This allows T_2 to be extracted from the signal exponential decay $\exp(-4\tau/T_2)$. Figure 3 shows the temperature evolution of the dephasing time for both stretching modes of the dimer. The evolution of the monomer time T_2[29] is also included for comparison.

The temperature evolution of the coherence time shows that the behavior of both stretching modes of the dimer is strongly different from that observed in the monomer species. This reveals different mechanisms from that found in our previous studies on DCl monomers in solid nitrogen[29] where a coupling between the DCl vibration and a local phonon of 19 cm^{-1} was highlighted. For the DCl dimer, the activation energy deduced from the temperature evolution of the dephasing time is too small (8 ± 3 and 5 ± 4 cm^{-1} for ν_1 and ν_2, respectively) to be easily related to the coupling with any local mode, even for the free mode ν_1. The influence of the nitrogen cage on the two oscillators of the dimer is weaker than that on the DCl stretching mode of the monomer.

Although the temperature evolution shows quite similar tendencies for both modes, the effect of the hydrogen bond is clearly observed whatever the temperature: the coherence time of the ν_2 band is always shorter than that of the ν_1 band. In the 7.5−20 K temperature range, the homogeneous line width of the ν_1 band increases from 0.19 to 0.50 cm^{-1}, whereas for the ν_2 band, it increases from 0.53 to 0.96 cm^{-1}. A significant part of the broadening of the vibrational mode involved in the hydrogen bond comes from dephasing processes.

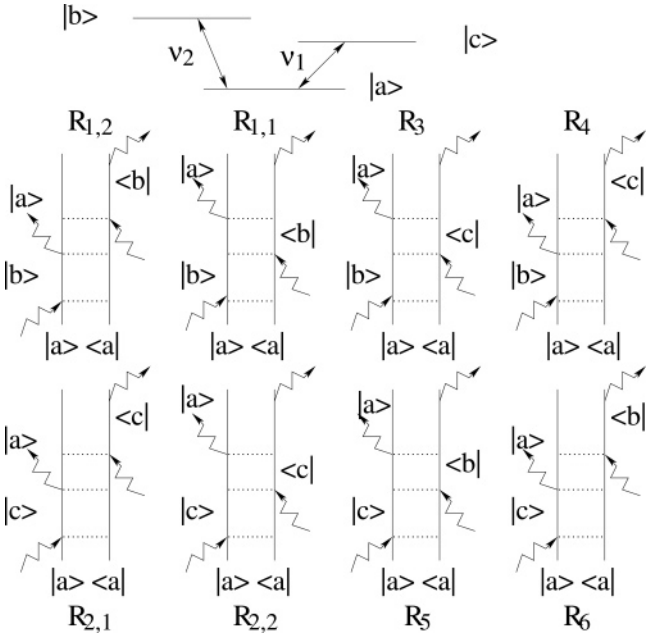

Figure 4. Double-sided Feynman diagrams for $P^{(3)}$ in the case of a three level system.

4. Model of the Nonlinear Signal

4.1. Theoretical Expression. The signals of interest have been obtained using a broad band excitation leading to the coherent excitation of several vibrational transitions. Both free and bonded D-Cl stretching modes of the dimers have to be taken into account. The recorded time-resolved signal $S(\tau)$ is related to the third-order polarization of the sample created by the interaction between the molecules and three time-delayed laser pulses, with a tunable delay τ between the first two pulses and a fixed delay T_w (the waiting time) between the last two pulses:

$$S(\tau) = \int_0^\infty |P^{(3)}(t,\tau)|^2 \, dt \tag{1}$$

Our specific setup allows to perform two pulse photon echo (TPE) experiments ($T_w = 0$) as well as stimulated three pulse photon echo (SPE) experiments ($T_w = nT_r$ with $T_r = 16$ ns), depending how the vibrational population lifetimes of the molecular system scale with T_r.[8] All of the characteristic times of the molecular dynamics are longer than the laser pulse duration; therefore, the laser pulses are considered as Dirac pulses in the following analysis. The coherent excitation of the dimer modes ν_1 and ν_2 are described here. The third-order polarization involves eight different contributions. They are represented by the eight Feynman's diagrams of Figure 4 in the case $\tau > 0$. The response functions corresponding to these diagrams can be summarized by the following expressions:[4]

$$C_i = R_{1,i} + R_{2,i} = \mu_i^4 e^{-i\omega_i(t-\tau)} e^{-\gamma_i(t+\tau)} [e^{-T_w/T_{1,i}} + e^{-T_w/T_g}] \tag{2}$$

$$C_3 = R_3 + R_4 = \mu_1^2 \mu_2^2 e^{-i(\omega_2 t - \omega_1 \tau)} e^{-(\gamma_2 t + \gamma_1 \tau)} [e^{-T_w/T_3} e^{-i(\omega_2 - \omega_1)T_w} + e^{-T_w/T_g}] \tag{3}$$

$$C_4 = R_5 + R_6 = \mu_1^2 \mu_2^2 e^{-i(\omega_1 t - \omega_2 \tau)} e^{-(\gamma_1 t + \gamma_2 \tau)} [e^{-T_w/T_3} e^{i(\omega_2 - \omega_1)T_w} + e^{-T_w/T_g}] \tag{4}$$

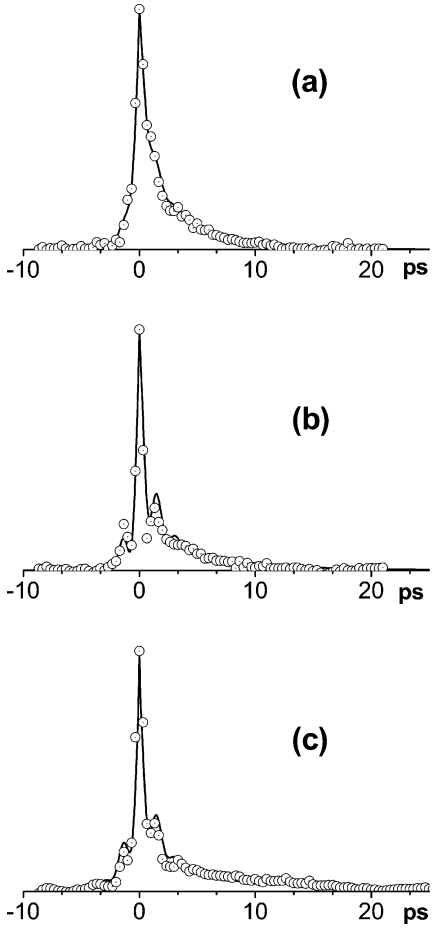

Figure 5. DFWM signals: experimental data (dots) and simulation (solid line); (a) [DCl] = 0.9%, T = 10 K, excitation centered at 2036 cm^{-1}, simulation: $p_2/p_1 = 2.3$, $p^{nodif} = 0.4$, (b) same sample and temperature, excitation centered at 2047 cm^{-1}, simulation: $p_2/p_1 = 1.2$, $p^{nodif} = 0.4$, (c) same concentration, T = 8 K, excitation centered at 2053 cm^{-1}, simulation: $p_2/p_1 = 0.5$, $p^{nodif} = 0.27$.

In the above equations, $i = 1$ or 2, μ_i, ω_i, γ_i, and $T_{1,i}$ represent the transition dipole moment, the frequency, the inverse of the dephasing time (T_2), and the population relaxation time of $v = 1$ of the mode ν_i, respectively; T_g represents the repopulation time of the ground state and T_3 the dephasing time of the mixed excitation of modes ν_1 and ν_2 (state $|b\rangle\langle c|$). This last time is in the picosecond range, as the dephasing times of both modes, so that the contribution of e^{-T_w/T_3} is effective only for TPE signals.

Obviously, only oscillations involving frequency differences $\delta = \omega_2 - \omega_1$ are clearly observed (Figure 5). It is why the oscillations due to the coherent excitation of the different isotopic species, such as those observed in the case of the study of the monomer,[29] are not described in this simplified analysis. Thus, the inhomogeneous frequency distribution of each mode may be taken into account as a broad profile including all the isotopic components. This description implies that all of the isotopic species are assumed to have the same characteristic times. The nonlinear response of the whole system involves eq 2−4 weighted by the inhomogeneous distribution. From the analysis of the absorption spectra (see part 3.1), the inhomogeneous distributions of ν_1 and ν_2 do not seem to be correlated and should be represented by two different functions. Therefore, the time dependence of the nonlinear response functions may be expressed as

$$Ctot_i = C_i(\langle\omega_i\rangle)\chi_i(t-\tau) \quad (5)$$

$$Ctot_3 = C_3(\langle\omega_1\rangle, \langle\omega_2\rangle)\chi_1(\tau)\chi_2(t) \quad (6)$$

$$Ctot_4 = C_4(\langle\omega_1\rangle, \langle\omega_2\rangle)\chi_2(\tau)\chi_1(t) \quad (7)$$

In the above equations, the inhomogeneous distributions are represented by $\chi_i(t)$ even real functions corresponding to the Fourier transform of the inhomogeneous profiles centered at zero and $\langle\omega_i\rangle$ represents the average value of the ν_i mode frequency.[4,34] To take into account the spectral profile of the laser pulse, each path described in Figure 4 is weighted by a function of p_i, where p_i represents the relative probability to excite the mode ν_i ($p_1 + p_2 = 1$).

4.1.1. TPE Signals ($T_w = 0$). If $\tau < 0$, no signal occurs. If $\tau > 0$, $T_w = 0$ in eq 2−4. The expression of the third-order polarization is

$$P^{(3)}(t,\tau > 0) \propto p_1^3 Ctot_1 + p_2^3 Ctot_2 + p_1^2 p_2 Ctot_3 + p_1 p_2^2 Ctot_4 \quad (8)$$

Oscillations involving δ frequency appear in the non rephasing part of the signal, at short τ delays, due to the short time range of $\chi_i(t)$.

4.1.2. SPE Signals ($T_w \neq 0$). A signal exists whatever the sign of τ. The expressions 5−7 can be applied with $\tau < 0$.[4,34] In our experiments, T_w is in the tens of nanoseconds so that $e^{-T_w/T_3} \simeq 0$ and the paths involving this expression are not taken into account. The waiting time is thus only included with the population relaxation times in real parameters which may be considered as weights A_j in the expressions of $Ctot_j$, $j = 1-4$, respectively: $A_{j=1,2} = e^{-T_w/T_{1,j}} + e^{-T_w/T_g}$, $A_3 = A_4 = A = e^{-T_w/T_g}$. The time-resolved signal is expressed as

$$P^{(3)}(t,\tau) \propto e^{-\gamma_1(t+\tau)}[p_1^3\mu_1^4 A_1\chi_1(t-\tau) + p_2^3\mu_2^4 A_2\chi_2(t-\tau)e^{-i\langle\delta\rangle(t-\tau)}e^{-\epsilon(t+\tau)} + A\mu_1^2\mu_2^2[p_1^2 p_2 e^{-i\langle\delta\rangle t}e^{-\epsilon(t)} + p_1 p_2^2 e^{i\langle\delta\rangle\tau}e^{-\epsilon\tau}]]e^{-i\langle\omega_1\rangle(t-\tau)} \quad (9)$$

with $\langle\delta\rangle = \langle\omega_2\rangle - \langle\omega_1\rangle$ and $\epsilon = \gamma_2 - \gamma_1$. The above equation describes the SPE signal $P_0^{(3)}$ obtained in the simplest case when no spectral diffusion occurs. In our experiments, the spectral diffusion is due to vibrational energy transfers (V−V transfers) between the guest molecules. Its influence is only taken into account during the waiting time.[8,34] When V−V transfers between the trapped dimers (quasiresonant V−V transfers) occur in times much shorter than T_w, the third-order polarization ($P_d^{(3)}$) has an expression written as eq 9 where the functions $\chi_i(t-\tau)$ are replaced by $\chi_i(t)\chi_i(\tau)$.[34] In fact, nonresonant energy transfers between the two modes inside the dimer are excluded in this expression of $P_d^{(3)}$. This case may be included in the description of $P_d^{(3)}$ with a modification of the A_j ($j = 1-4$) parameters: taking into account a probability that intra-dimer V−V transfer changes the excited state during the waiting time, only the weight of $\exp^{-T_w/T_{1,i}}$ ($i = 1, 2$) in A_j is modified.

To get a simple approach of the experimental signals, we will describe the third-order polarization by

$$P_{tot}^{(3)}(t,\tau) = p^{nodif}P_0^{(3)}(t,\tau) + (1 - p^{nodif})P_d^{(3)}(t,\tau) \quad (10)$$

where $P_0^{(3)}$ and $P_d^{(3)}$ are third-order polarizations with no spectral diffusion and with very efficient spectral diffusion

respectively, and p^{nodif} is the probability that no spectral diffusion occurs during the waiting time.

4.2. Analysis of Nonlinear Signals. As previously noticed, the long component reflects the behavior of dephasing times, so that γ_i parameters can be fixed to the values given in Figure 3, obtained from the signals involving almost only one of the stretching modes. The following analysis is mainly focused on the behavior of the short component, to extract the complementary information on the vibrational dynamical processes.

The short component comes necessarily from SPE signals whereas the long one may be due to TPE or SPE signals. If the long component was mainly due to TPE, then the negative part of $S(\tau)$ would reflect only a fast spectral diffusion process ($p^{nodif} \sim 0$ in eq 10). Assuming such a case, the simulated signals exhibit very asymmetric oscillations at short delay and cannot reproduce the experimental data. Therefore, the influence of TPE signals seems negligible. A rephasing process is thus always observed in the SPE signals upon the excitation of one or the other mode of the dimer. It means that the V−V transfer characteristic times are always at least of the same order of magnitude as T_w, i.e., in the tens of nanoseconds.

The experimental results are fitted using eqs 10 and 1. Few parameters are fixed, in addition to γ_i. $\chi_i(t)$ is adjusted on the Fourier transform of the absorption spectra at low temperature for both frequency ranges,[36] using an analytic expression of the form: $\chi(t) = \alpha e^{-|t|/a} + \beta e^{-|t|/b}$. For $\chi_1(t)$, $a = 2.06\ 10^{-2}$ ps, $b = 2.44$ ps, $\alpha/\beta = 0.15$; for $\chi_2(t)$, $a = 1.19$ ps, $b = 8.33$ ps, $\alpha/\beta = 10$. For each DFWM signal, a first estimation of p_i is deduced from the laser frequency. Oscillations around $\tau = 0$ appear more or less clearly, depending on the mean laser frequency, according to the influence of p_i in eq 10. The contrast of these oscillations is also influenced by parameters A_j, with a maximum for $A_1 = A_2 = A$.

As shown in Figure 5, a good agreement between simulation and experiments is obtained within the above description. The long components are well reproduced whatever the laser frequency. Unfortunately, experimental data are not precise and numerous enough to conclude on the exact relative values of parameters A_j for each nonlinear response. Nevertheless, the data are correctly simulated with $A_1 = A_2 = 2A$, corresponding to the case $T_{1,i} \gg T_w = T_r = 16ns$. Whatever the temperature, p^{nodif} is always found ~ 0.4, except for a laser frequency close to the DCl monomer absorption where p^{nodif} decreases down to 0.25 (Figure 5c). In this last case, the nonlinear response of monomers also influences the short component. In the range of concentration ($\sim$1%) used in the experiments, the spectral diffusion is the main observed process under the excitation of monomers. According to the results and estimations given in ref 29, a value of $p^{nodif} < 10^{-4}$ is expected for the nonlinear response of the monomer. The excitation of a fraction of monomers enhances the short component, reducing p^{nodif} in the simulations. The value of p^{nodif} corresponding to the effect of V−V transfer between the dimers is thus given by the previous value of 0.4 ($\pm$0.03).

5. Discussion

5.1. Population Relaxation Times. Population relaxation times are not measured directly in our experiments. A lower limit is obtained indirectly from the analysis of TPE and SPE signals (part. 4.2). TPE signals are clearly observed when both population relaxation times (T_1 and T_g) are shorter than the waiting time $T_r = 16$ ns. The analysis of time-resolved results on $(DCl)_2/N_2$ shows that the contribution of TPE signals is negligible, so that at least, $T_g > 16$ ns. In contrast, TPE signals were observed in our experiments on $(DCl)_3$ trapped in solid N_2[35]: this result is consistent with a vibrational relaxation in the trimer faster than in the dimer, as observed in jet experiments where a value of $T_1 = 1.3$ ns was reported for $(HCl)_3$.[37] In the gas phase, the times T_1 for both H−Cl stretching modes of $(HCl)_2$ are significantly longer than 16 ns,[18,22] whereas only a lower limit of 3 ns was measured for $(DCl)_2$.[19] By means of slit jet experiments on $(HF)_2$ and $(DF)_2$,[38] Davis et al. observed an enhancement of T_1 from $(HF)_2$ to $(DF)_2$, assigned to a deuteration effect. By comparison, the relaxation times of $(DCl)_2$ are expected to be longer than those of $(HCl)_2$, in agreement with the present analysis of DFWM signals assuming $T_1 > 16$ ns.

5.2. V−V Transfers. Nonresonant intermolecular vibrational energy transfer also contributes to the loss of vibrational coherence and is responsible for the spectral diffusion, occurring on a nanosecond time scale. The rate of V−V transfer between two guest molecules depends on the intermolecular distance and the energy mismatch.[39,40] In the case of dimers, nonresonant V−V transfer can occur between two distant dimers but also between the two intramolecular D-Cl stretching modes inside a dimer.

In this last case, a fast transfer rate is expected due to the short distance between both oscillators. Owing to the near perpendicular geometry of the dimer, the dipole−dipole and dipole−quadrupole interactions are weakened, so that the major contribution to the transfer rate results from the quadrupole-quadrupole term. For resonant transfer, the rate is written as

$$k_{QQ} = \frac{\chi_{QQ}{}^2 |Q_1|^2 |Q_2|^2}{n^4 p^2 \gamma_a R^{10}} \qquad (11)$$

$R = 3.54$ Å is the distance between the two DCl molecules in the dimer,[24] $\gamma_a = (\gamma_1 + \gamma_2)/2$ is the mean homogeneous width of the two D-Cl stretching modes, n is the refractive index of solid nitrogen, $\chi_{QQ}{}^2$ is a parameter depending on the geometry of the dimer,[41] and Q_i is the transition quadrupole moment of the mode ν_i of $(DCl)_2$. The transition quadrupole moment of HCl is quite large: $|Q| = 0.354$ D Å.[42] Assuming a similar value for the stretching modes of $(DCl)_2$, eq 11 gives $k_{QQ} \geq 1$ ps^{-1}. However, the energy gap between the two D-Cl stretching modes is large (≈ 20 cm^{-1}) so that the nonresonant energy transfer between the two modes is phonon-assisted. If these transfers occurred in less than 10 ns, then the rephasing process could not be observed in contradiction with the described DFWM experiments. Consequently, the coupling between phonons and D-Cl modes should be weak enough to reduce the transfer rate by at least 4 orders of magnitude compared to the resonant case.

Comparatively, V−V transfers between randomly oriented isolated dimers are mainly due to dipole − dipole interactions. To estimate V−V transfer rates, calculations similar to those described in ref 29 in the case of DCl monomers can be done. For each mode i, one can define a characteristic time T^{VV} of V−V transfer related to the probability that no transfer has occurred before the time t after the excitation of population: $\eta(t) = \exp[-(t/T^{VV})^{1/2}]$. On one hand, T^{VV} is measured in DFWM experiments by the probability $\eta(t = T) = p^{nodif}$ (cf eq 10).[29] $T^{VV} \simeq 19 \pm 3$ ns is obtained in the region of ν_2, where the influence of the nonlinear response of the monomer is negligible. On the other hand, T^{VV} is calculated using the following data: the homogeneous bandwidth (γ_i) extracted from DFWM signals, the inhomogeneous distribution of ν_i frequencies ($g_i(\nu)$) simulated as a sum of four Lorentzian bands from

the absorption spectra (cf. part 3.1), the transition dipole moment (μ_i) with $|\mu_2| = 1.2|\mu_1|$[28] and the concentration of DCl-D(H)Cl dimers (c_d) estimated from the absorption band intensities ($c_d = 0.57\%$ in the samples of interest).[43] Using $|\mu_1| = |\mu_{DCl-gas}| = 0.056$ D,[44] $T^{VV} = 360-280$ ns and $T^{VV} = 280-240$ ns are obtained in the 7.5−20 K temperature range, for modes ν_1 and ν_2, respectively. To reach a satisfactory agreement with the value estimated from the DFWM signals ($T^{VV} = 19$ ns), an enhancement of the transition dipole moment $|\mu_1|$ due to the nitrogen environment has to be assumed in the calculations ($T^{VV} \propto |\mu|^{-4}$): $|\mu_1| \simeq 2|\mu_{DCl-gas}|$. A similar conclusion was deduced from monomers study.[29,35] The weak temperature dependence of T^{VV} is related to the homogeneous-inhomogeneous bandwidths ratio of 0.1 to 0.4, corresponding to a case of a low sensitivity of T^{VV} to γ_i, as was shown in ref 29.

5.3. Coherence Time. The analysis of the DFWM signals proves that the vibrational population lifetime is greater than the waiting time T_r and thereby, $T_2^* \simeq T_2$, with values and temperature dependence reported in Figure 3.

As mentioned above, a coupling between the two intramolecular stretching modes and a lattice mode cannot explain the temperature behavior of the coherence times. Their quasi-similar evolution as a function of temperature is quite surprising. Indeed, the behavior of the coherence time for the mode ν_1 is expected to be the same as for the monomer,[29] because this intramolecular vibration is not fully involved in the hydrogen bond, with an hydrogen motion exploring the nitrogen environment.

At this stage, it is interesting to compare our results with the experiments performed by Bonn et al.[45] in zeolite catalysts. With transient IR hole-burning spectroscopy, the authors observed large variations in the pure dephasing times of the ν(O−D) stretching mode of differently hydrogen-bonded surface hydroxyls. Two kinds of hydrogen bonded O−D vibrations have been investigated: one represented by OD groups hydrogen bonded to zeolite lattice oxygen atoms (OD...O) and the other constituted by OD...N_2 hydrogen bonded, the nitrogen molecule being adsorbed on the surface of the zeolite cage. Whereas these two OD groups are involved in hydrogen bonds of the same strength, with the same ν(O−D) population lifetimes, they exhibit very different temperature dependence of T_2^*. For OD···N_2, the dephasing time seems to be temperature independent, while for OD···O, T_2^* decreases exponentially with the temperature, with an activation energy showing the coupling to zeolite lattice modes. This very large difference is related to the shape of the hydrogen bond potentials. In the case of the OD···O groups, the (OD−O) potential is governed by the geometry of the zeolite lattice whereas the (OD−N_2) potential is strongly anharmonic, governed by the hydrogen bond, and reveals the coupling between ν(O−D) and the low-frequency intermolecular hydrogen bridge stretching mode.

The mode ν_2 of DCl dimers can be reasonably compared to the mode ν(O−D) of the OD···N_2 group because it is involved in the hydrogen bond of the dimer. In both cases, the coupling with the hydrogen bond intermolecular stretching mode seems stronger than the coupling with the surrounding lattice and the evolution with the temperature is weak (in the narrow temperature range explored). On the contrary, the lattice clearly influences the dephasing process of ν(O−D) in the OD···O group, as was observed for DCl monomers in nitrogen solid, where no hydrogen bond was involved.

The case of the free mode ν_1 is more intriguing. In fact, it has an intermediate behavior between those of the monomer and of ν_2, but within the experimental errors, the temperature dependence of its dephasing time could be the same as for ν_2. It seems that the complexation isolates the vibration from the nitrogen cage. This assumption is reinforced by recent experiments on DCl embedded in mixed N_2/Ar matrixes[35] where the coherence time of ν_1 in the complex $(DCl)_2$···N_2 is shorter than that of the complex DCl···N_2. So, the behavior of the free mode ν_1 is also influenced by the hydrogen bond.

This result can be discussed qualitatively. The dephasing time is related to two physical parameters, the mean amplitude of the modulation of the vibrational frequency, D, and the time scale of this modulation, τ_c. In the case of a hydrogen bonded system, the description of these parameters involves the characteristics of the hydrogen bridge stretching mode and its coupling with the probed vibrational mode. Following the model developed by Robertson and Yarwood,[14] well adapted to the results obtained by Bonn et al., τ_c only depends on the hydrogen bond frequency and its coupling to the bath, whereas D depends on the strength of the coupling between the intramolecular mode and the hydrogen bond. If the influence of the hydrogen bond is considered as the most important dephasing process for ν_1, the main difference between ν_1 and ν_2 is the strength of this coupling, leading to values of T_2^* higher for ν_1 than for ν_2, as it is observed, but also to similar temperature dependence of the dephasing process because the same hydrogen bond affects the two vibrations. Unfortunately, our results are not precise enough to conclude on this last point.

6. Conclusion

$(DCl)_2$ in solid N_2 is a simple model system appropriate to an investigation of the effect of a weak hydrogen bond on the vibrational motion. Time-resolved one color degenerate four wave mixing experiments with the FEL have allowed to explore the dynamics of the two D-Cl stretching intramolecular modes. Valuable information on their population relaxation times, on their coherence times and on V−V transfers has been obtained.

Population relaxation times in the dimer remain longer than the tens of nanoseconds in the solid, i.e., much longer than that of the trimer, measured in the gas phase:[37] fast relaxation paths to low energy modes are closed. V−V transfer is also a long dynamical process, the energy transfer from one stretching mode to the other inside the dimer is quite inefficient. On the other hand, the analysis of V−V transfer from the DFWM signals is consistent with the estimation of the V−V transfer rate between different guest dimers in the sample with the assumption of an enhancement of the transition dipole moment of DCl by the nitrogen lattice, suggested by the experiments on the monomers.[29]

The dephasing process has the shortest dynamics and, as usual, is the most sensitive to the environment. The environment effects are first observed through the frequency shifts of the vibrational transitions: the gas-to-matrix shift, the shift from the monomer to the dimer and the shift from the free to the bonded mode, corresponding to various deformations of the D-Cl intramolecular potential. Whereas the gas-to-matrix shift is the same for the monomer and for both stretching modes of the dimers, the influence of the lattice on the vibrational coherence is strongly different from the monomer to the dimer. Our results show that the dephasing processes in the dimer are related to the hydrogen bond which affects more strongly the mode ν_2 than the mode ν_1. As the gas-to-matrix shift in nitrogen is very similar to the shift between the bonded mode and the monomer frequencies, an influence of the lattice on the coherence time is also expected. Such an effect can be observed through the study of $(DCl)_2$ in various environments. We have

recently obtained some results in argon matrixes which highlight the effect of the nitrogen environment on the vibrational coherence of D−Cl, even for the dimers.[35]

Acknowledgment. The authors gratefully acknowledge J. M. Ortéga and the members of the CLIO group of the LURE laboratory, especially F. Glotin and R. Andouart, for their helpful assistance with the experiments.

References and Notes

(1) Oxtoby, D. W. *Adv. Chem. Phys.* **1979**, *40*, 1.
(2) Galaup, J.-P. In *Advances in Multiphoton Processes and Spectroscopy*; Lin, S. H., Villaeys, A. A., Fujimura, Y., Eds.; World Scientific: Singapore, 2004; Vol. 16, Chapter 2, pp 73−248.
(3) Wright, J. C. *Int. Rev. Phys. Chem.* **2002**, *21*, 185.
(4) Mukamel, S. *Principles of Nonlinear Optical Spectroscopy*; Oxford University Press: New York, 1995.
(5) Zimdars, D.; Tokmakoff, A.; Chen, S.; Greenfield, S. R.; Fayer, M. D. *Phys. Rev. Lett.* **1993**, *70*, 2718.
(6) Stenger, J.; Madsen, D.; Dreyer, J.; Hamm, P.; Nibbering, E. T.; Elsaesser, T. *Chem. Phys. Lett.* **2002**, *354*, 256.
(7) Galaup, J. P.; Broquier, M.; Crépin, C.; Dubost, H.; Ortéga, J. M.; Chaput, F.; Boilot, J. P. *J. Lumin.* **2000**, *86*, 363.
(8) Crépin, C.; Broquier, M.; Dubost, H.; Galaup, J. P.; Le Gouët, J. L.; Ortéga, J. M. *Phys. Rev. Lett.* **2000**, *85*, 964.
(9) Maréchal, Y.; Witkowsky, A. *J. Chem. Phys.* **1968**, *48*, 3697.
(10) Blaise, P.; Wojcik, M. J.; Henri-Rousseau, O. *J. Chem. Phys.* **2005**, *122*, 064306 and references therein.
(11) Rösch, N.; Ratner, M. A. *J. Chem. Phys.* **1974**, *61*, 3344.
(12) Bratos, S.; Rios, J.; Guissani, Y. *J. Chem. Phys.* **1970**, *52*, 439.
(13) Bratos, S. *J. Chem. Phys.* **1975**, *63*, 3499.
(14) Robertson, G. N.; Yarwood, *J. Chem. Phys.* **1978**, *32*, 267.
(15) Rank, D. H.; Rao, B. S.; Wiggins, T. A. *J. Chem. Phys.* **1962**, *37*, 2511.
(16) Rank, D. H.; Sitaram, P.; Glickman, A.; Wiggins, T. A. *J. Chem. Phys.* **1963**, *39*, 2673.
(17) Ohashi, N.; Pine, A. S. *J. Chem. Phys.* **1984**, *81*, 73.
(18) Schuder, M. D.; Lovejoy, C. M.; Lascola, R.; Nesbitt, D. J. *J. Chem. Phys.* **1993**, *99*, 4346.
(19) Schuder, M. D.; Nelson, D. D.; Nesbitt, D. J. *J. Chem. Phys.***1993**, *99*, 5045.
(20) Schuder, M. D.; Nesbitt, D. J. *J. Chem. Phys.* **1994**, *100*, 7250.
(21) Farnik, M.; Davis, S.; Nesbitt, D. *J. Faraday Discuss.* **2001**, *118*, 63.
(22) Ni, H.; Serafin, M.; Valentini, J. J. *J. Chem. Phys.* **2000**, *113*, 3055.
(23) Perchard, J. P.; Cipriani, J.; Sivi, B.; Maillard, D. *J. Mol. Struct.* **1983**, *100*, 317.
(24) Girardet, C.; Maillard, D.; Schriver, A.; Perchard, J. P. *J. Chem. Phys.* **1979**, *70*, 1511.
(25) Maillard, D.; Schriver, A.; Perchard, J. P.; Girardet, C. *J. Chem. Phys.* **1979**, *71*, 505.
(26) Maillard, D.; Schriver, A.; Perchard, J. P.; Girardet, C. *J. Chem. Phys.* **1979**, *71*, 517.
(27) Maillard, D.; Schriver, A.; Perchard, J. P.; Girardet, C.; Robert, D. *J. Chem. Phys.* **1977**, *67*, 3917.
(28) Perchard, J. P.; Maillard, D.; Schriver, A.; Girardet, C. *J. Raman Spectrosc.* **1981**, *11*, 406.
(29) Broquier, M.; Crépin, C.; Cuisset, A.; Dubost, H.; Galaup, J. P.; Roubin, P. *J. Chem. Phys.* **2003**, *118*, 9582.
(30) Prazeres, R.; Glotin, F.; Insa, C.; Jaroszynski, D. A.; Ortéga, J. M. *Eur. Phys. J. D* **1998**, *3*, 87.
(31) Glotin, F.; Ortéga, J. M.; Prazeres, R.; Rippon, C. *Nucl. Instrum. Methods B* **1998**, *144*, 8.
(32) Crépin, C.; Broquier, M.; Cuisset, A.; Dubost, H.; Galaup, J. P.; Ortéga, J. M. *Nucl. Instrum. Methods Phys. Res. A* **2004**, *528*, 636.
(33) An inhomogeneous broadening due to dipole−dipole interactions produces a Lorentzian profile of the absorption band (Stoneham, A. M. *Rev. Mod. Phys.* **1969**, *41*, 82) and such a model was used in the study of DCl monomers in solid nitrogen, ref 29.
(34) Crépin, C. *Phys. Rev. A* **2003**, *67*, 13401.
(35) Cuisset, A. Ph.D. Thesis, Université Paris-Sud, Paris, France, 2003.
(36) From spectral analysis, inhomogeneous broadening dominates the absorption profile.
(37) Farnik, M.; Nesbitt D. J. *J. Chem. Phys.* **2004**, *121*, 12386.
(38) Davis, S.; Anderson, D. T.; Farell, J. T. Jr.; Nesbitt, D. J. *J. Chem. Phys.* **1996**, *104*, 8197.
(39) Lyo, S. K. *Phys. Rev. B* **1980**, *22*, 3616.
(40) Harig, M.; Charneau, R.; Dubost, H. *Phys. Rev. Lett.* **1982**, *49*, 715.
(41) Dexter, D. L. *J. Chem. Phys.* **1953**, *21*, 836.
(42) From the theoretical value of $\partial Q/\partial R$ in Nesbet, R. K. *J. Chem. Phys.* **1964**, *41*, 100.
(43) Assuming a statistical distribution of the guest molecules and $|\mu_1| = |\mu_{\text{monomer}}|$, the effective concentration of all of the dimers (c_{eff}) is related to the intensity ratio (I) between the integrated absorption of the band associated to mode ν_1 and that of the monomer over all of the absorption spectrum including hydrogenated and deuterated species by $c_{\text{eff}} = (I^2/12+I)$; c_d is obtained when the ratio of deuterated species is applied to c_{eff}.
(44) Smith, F. G. *J. Quant. Spectrosc. Rad. Trans.* **1972**, *13*, 717.
(45) Bonn, M.; Brugmans, M. J. P.; Kleyn, A. W.; Van Santen, R. A.; Bakker, H. J. *Phys. Rev. Lett.* **1996**, *76*, 2440.